# ISOSPIN FRACTIONATION IN NUCLEAR MULTIFRAGMENTATION

H.S. Xu[a], M.B. Tsang[a], T.X. Liu[a], X.D. Liu[a], W.G. Lynch[a], W.P. Tan[a], G. Verde[a], A. Vander Molen[a], A. Wagner[a], H.F. Xi[a], C.K. Gelbke[a], L. Beaulieu[b], B. Davin[b], Y. Larochelle[b], T. Lefort[b], R.T. de Souza[b], R. Yanez[b], V. Viola[b], R.J. Charity[c], and L.G. Sobotka[c]

To explore isospin fractionation, $^{112}$Sn+$^{112}$Sn, $^{112}$Sn+$^{124}$Sn, $^{124}$Sn+$^{112}$Sn and $^{124}$Sn+$^{124}$Sn collisions were studied by bombarding $^{112}$Sn and $^{124}$Sn targets of 5 mg/cm$^2$ areal density with 50 MeV per nucleon $^{112}$Sn and $^{124}$Sn beams from the K1200 cyclotron in the National Superconducting Cyclotron Laboratory at Michigan State University. Isotopically resolved particles with $1 \le Z \le 10$ were detected with nine telescopes of the Large Area Silicon Strip Array (LASSA). The center of the LASSA device was located at a polar angle of $\theta = 32°$ with respect to the beam axis, covering polar angles of $7° \le \theta \le 58°$. Impact parameter selection was provided by the multiplicity of charged particles [1] measured with LASSA and with 188 plastic scintillator - CsI(Tl) phoswich detectors of the Miniball/Miniwall array [2]; the combined apparatus covered 80% of the total solid angle. Central collisions were selected by gating on the top 4% of the charged-particle multiplicity distribution, corresponding to a reduced impact parameter of $b/b_{max} \le 0.2$ in the sharp cut-off approximation [3]. Previous studies demonstrate that such collisions lead to bulk multifragmentation [4].

Figure 1 shows carbon-isotope particle-identification histograms [5], integrated over all LASSA telescopes for central $^{112}$Sn+$^{112}$Sn (left panel) and $^{124}$Sn+$^{124}$Sn (right panel) collisions. The isotopes from $^{11}$C to $^{15}$C are well resolved. The centroid of the mass distribution for the neutron-rich $^{124}$Sn+$^{124}$Sn system is shifted by about 1/2 mass unit towards heavier isotopes compared to that for $^{112}$Sn+$^{112}$Sn. The background in the spectrum arises from coincidence summing of signals from light particles and neutrons in the CsI(Tl) scintillators. For particles stopped in the Si detectors, the background is negligible[6].

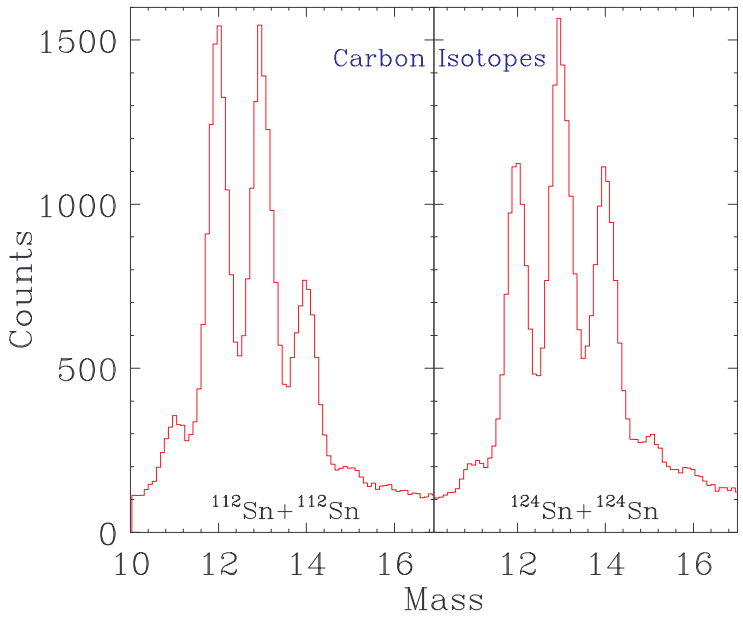


Figure 1: Carbon isotope particle identification histograms obtained for $^{112}$Sn+$^{112}$Sn (left panel) and $^{124}$Sn +$^{124}$Sn (right panel) reactions.

A basic framework for the extraction of free neutron and proton densities at breakup from isotopic ratios has been provided in ref. [7,8]. Assuming chemical equilibrium [8], one can write the primary multiplicity (before secondary decay of excited states) for an isotope with neutron number, *N*, and proton number, *Z*, in its i-th state as:

$$M_i(N,Z) \propto V(2J_i+1)\cdot e^{(N\mu_n+Z\mu_p+B(N,Z)-E_i^*)/T} \propto V(2J_i+1)\cdot \rho_n^N \cdot \rho_p^Z \cdot e^{B(N,Z)/T}\cdot e^{-E_i^*/T} \qquad (1)$$

where *V* is the volume, $\rho_n = M_i(1,0)/V$ and $\rho_p = M_i(0,1)/V$ are the primary free neutron and free proton densities respectively; *B(N,Z)*, $J_i$, and $E_i$* are the ground state binding energy, spin, and excitation energy of the isotope in the i-th state; $\mu_n$ and $\mu_p$ are the neutron and proton chemical potentials and *T* is the temperature. Secondary decay of excited fragments after breakup introduces corrections to the final yields. The leading order correction arises from particle stable states and is a multiplicative factor, $\tilde{z}_{N,Z}(T) = \sum_{i,stable}(2J_i+1)\cdot e^{-E_i^*/T}$, where the sum is over particle stable states of the fragment. We further assume that the correction due to particle unstable decay can be represented by another multiplicitive factor $f_{N,Z}(T)$:

$$M_{obs}(N,Z) \propto V\cdot \rho_n^N \cdot \rho_p^Z \cdot e^{B(N,Z)/T}\cdot \tilde{z}_{N,Z}(T)\cdot f_{N,Z}(T) \qquad (2)$$

In principle, the influence of $\tilde{z}_{N,Z}(T)$ and $f_{N,Z}(T)$ can be assessed by model calculations.

The ratio of the multiplicities of neighboring mirror nuclei is related to the ratio of the free neutron and proton densities by:

$$\frac{M_{obs}(Z,N)}{M_{obs}(N,Z)} = \frac{\tilde{z}_{Z,N}(T)\cdot f_{Z,N}(T)}{\tilde{z}_{Z,N}(T)\cdot f_{N,Z}(T)}\cdot\frac{\rho_n}{\rho_p}\cdot e^{\Delta B/T} \approx \frac{\rho_n}{\rho_p}\cdot e^{\Delta B/T}\,\frac{f_{Z,N}(T)}{f_{N,Z}(T)}, \qquad (3)$$

where *ΔB=B(Z,N)-B(N,Z)* is the binding energy difference between the two mirror nuclei and *N=Z-1*. The similarity between the excited particle stable states of the two mirror nuclei leads to an approximate cancellation of the partition functions $\tilde{z}_{N,Z}(T)/\tilde{z}_{N,Z}(T)$~1.

More relevant for the investigation of isotopic effects is the construction of observables which maximize the sensitivity to isospin effects and minimize the sensitivity to temperature and sequential decays. Extensive studies indicate that distortions from sequential decays are specific to each isotope ratio and depend less on entrance channel [9-11]. To test for an enhanced N/Z ratio of the gas phase, we compare the free neutron and free proton densities obtained from Eq. 1 and 2 for the four Sn+Sn systems. Distortions from sequential decays are minimized by normalizing the isotopic and isotonic ratios to those of the $^{112}$Sn+$^{112}$Sn system, giving a relative free neutron density,

$$\left(\hat{\rho}_n\right)^k = \frac{M_{obs}(N_i+k,Z_i)}{M_{obs}(N_i,Z_i)} \Big/ \frac{M_{obs}^{112}(N_i+k,Z_i)}{M_{obs}^{112}(N_i,Z_i)} = \left(\frac{\rho_n}{\rho_n^{112}}\right)^k, \qquad (4)$$

and a relative free proton density,

$$\left(\hat{\rho}_p\right)^k = \frac{M_{obs}(N_i,Z_i+k)}{M_{obs}(N_i,Z_i)} \Big/ \frac{M_{obs}^{112}(N_i,Z_i+k)}{M_{obs}^{112}(N_i,Z_i)} = \left(\frac{\rho_p}{\rho_p^{112}}\right)^k. \qquad (5)$$

In these expressions, it has been assumed that temperature differences for the four systems (which have nearly the same center of mass energy per nucleon) are negligible[12], enabling the cancellations of both the binding energy factors and the partition functions. Cancellations of the particle unstable feeding corrections are also assumed[9-11].

Experimental values for $<\hat{\rho}_n>$ and $<\ddot{\rho}_p>$ were extracted for central collisions from isotope yields measured with good statistics and low background and listed in Table I. To reduce the sensitivity to projectile and target remnants, these data were further selected by a rapidity gate of $0.4 \leq y/y_{beam} \leq 0.65$, where y and $y_{beam}$ are the rapidities of the analysed particle and beam, respectively. The resulting mean values, $<\hat{\rho}_n>$ and $<\ddot{\rho}_p>$, extracted from isotope ratios for the four systems: $^{112}Sn+^{112}Sn$, $^{112}Sn+^{124}Sn$, $^{124}Sn+^{112}Sn$, $^{124}Sn+^{124}Sn$ are shown in Fig. 2 as a function of the N/Z ratio for the composite system, $(N/Z)_O$. The solid circles and squares denote values for $<\hat{\rho}_n>$ and $<\ddot{\rho}_p>$ extracted using Eq. 4 and 5 for k=1, the open circles and squares denote corresponding values for k=2 and the stars denote values for k=3. The error bars include both statistical errors, uncertainties arising from background subtraction and systematic errors. The excellent agreement between the extracted values obtained for k=1, 2 and 3 suggests that the factorization into neutron and proton densities in Eq. 1 and the cancellation of the secondary decay corrections in Eq. 4 and 5 are valid. The agreement between the mixed systems, $^{112}Sn(beam)+^{124}Sn(target)$ and $^{124}Sn(beam)+^{112}Sn(target)$, with $(N/Z)_O = 1.36$ reflects the fact that the kinematic distortions due to the acceptance of LASSA are negligible.

| Isotope Ratios $\Delta A=1$ | $\Delta A=2$ | $\Delta A=3$ | Isotone Ratios $\Delta Z=1$ | $\Delta Z=2$ | $\Delta Z=3$ |
|---|---|---|---|---|---|
| d/p | | | $^{3}He/d$ | | |
| t/d | t/p | | $^{4}He/t$ | | |
| $^{4}He/^{3}He$ | $^{6}He/^{4}He$ | $^{6}He/^{3}He$ | $^{7}Li/^{6}He$ | | |
| $^{7}Li/^{6}Li$ | | | $^{7}Be/^{6}Li$ | | |
| $^{8}Li/^{7}Li$ | $^{8}Li/^{6}Li$ | | $^{9}Be/^{8}Li$ | | |
| $^{9}Li/^{8}Li$ | $^{9}Li/^{7}Li$ | $^{9}Li/^{6}Li$ | $^{10}B/^{9}Be$ | $^{10}B/^{8}Li$ | |
| $^{10}Be/^{9}Be$ | $^{9}Be/^{7}Be$ | $^{10}Be/^{7}Be$ | $^{11}B/^{10}Be$ | $^{11}B/^{9}Li$ | |
| $^{11}B/^{10}B$ | | | $^{12}C/^{11}B$ | $^{12}C/^{10}Be$ | $^{12}C/^{9}Li$ |
| $^{12}B/^{11}B$ | $^{12}B/^{10}B$ | | $^{13}C/^{12}B$ | | |
| $^{13}B/^{12}B$ | $^{13}B/^{11}B$ | $^{13}B/^{10}B$ | $^{14}C/^{13}B$ | | |
| $^{13}C/^{12}C$ | | | $^{14}N/^{13}C$ | $^{14}N/^{12}B$ | |
| $^{14}C/^{13}C$ | $^{14}C/^{12}C$ | | $^{15}N/^{14}C$ | $^{15}N/^{13}B$ | |
| $^{15}N/^{14}N$ | | | $^{16}O/^{15}N$ | $^{16}O/^{14}C$ | $^{16}O/^{13}B$ |
| $^{16}N/^{15}N$ | $^{16}N/^{14}N$ | | $^{17}O/^{16}N$ | $^{17}O/^{15}C$ | |
| $^{17}N/^{16}N$ | $^{17}N/^{15}N$ | $^{17}N/^{14}N$ | $^{18}O/^{17}N$ | | |
| $^{17}O/^{16}O$ | | | | | |
| $^{18}O/^{17}O$ | $^{18}O/^{16}O$ | | | | |

Table I: List of isotope and isotone ratios used in the present work.

If the relative concentrations of neutrons and protons were the same throughout each system and the overall nuclear matter density was independent of $(N/Z)_O$, the relative free neutron and proton densities as functions of $(N/Z)_O$ would follow the solid and dashed lines in Fig. 2, respectively. The experimental data shows that as $(N/Z)_O$ increases, the system responds by making the asymmetry of the

gas (given by the ratio $<\hat{\rho}_n>/<\ddot{\rho}_p>$ ) much greater than the asymmetry of the total system (given by the ratio of solid to dashed lines).

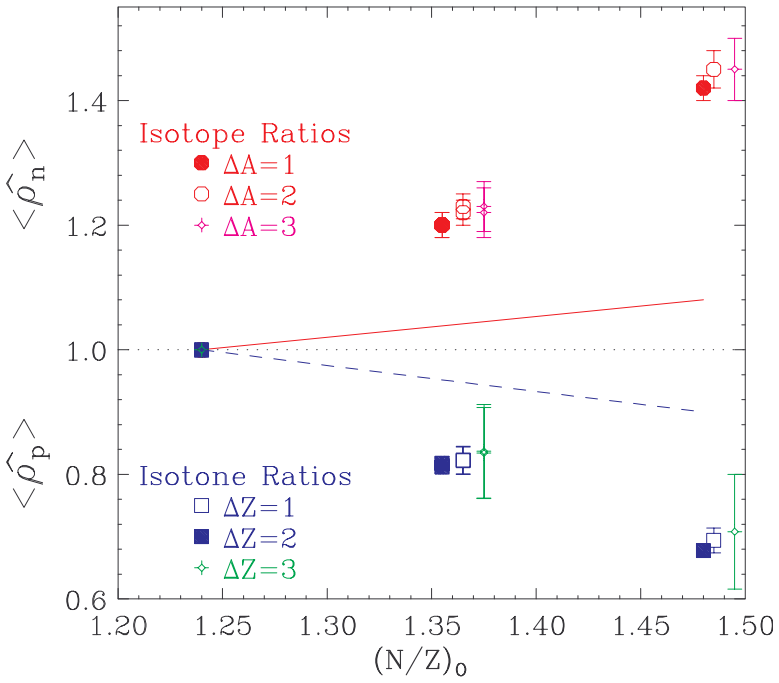


Figure 2: The mean relative free neutron and free proton density (Eq. 6 and 7) as a function of $(N/Z)_o$. The solid and dotdashed lines are the expected n-enrichment and p-depletion with the increase of isospin of the initial systems.

While this analysis of $<\hat{\rho}_n>$ and $<\ddot{\rho}_p>$ demonstrates the neutron enrichment of the free nucleonic gas, it does not provide absolute values for $\rho_n/\rho_p$[13]. To estimate $\rho_n/\rho_p$ using Eq. 3, three pairs of mirror nuclei, $^3$H/$^3$He, $^7$Li/$^7$Be and $^{11}$C/$^{11}$B were analyzed for the $^{112}$Sn+$^{112}$Sn and $^{124}$Sn+$^{124}$Sn systems. The solid points in Figure 3 show the isobaric yield ratios of these mirror nuclei as a function of the binding energy difference, $\Delta B$. The data display a trend similar to Eq. 3, but differ in details, possibly due to Coulomb effects and the secondary decay factor $f_{Z,N}(T)/f_{N,Z}(T)$ which have been neglected. Assuming the correction to the individual ratios due to the secondary decay factor $f_{Z,N}(T)/f_{N,Z}(T)$to be random and larger than the experimental uncertainties, extrapolating to vanishing $\Delta B$ via the solid lines yields values, following Eq. 3, for $\rho_n/\rho_p$ of 2.5 for the $^{112}$Sn+$^{112}$Sn system (left panel) and 5.5 for the $^{124}$Sn+$^{124}$Sn system (right panel). Secondary decay calculations using SMM models [14,15], which do not reproduce the detail features of the isotopic distributions, predict that such extrapolations may underestimate $\rho_n/\rho_p$ by as much as 30-50%. Alternative extrapolations, denoted by the dashed and dot-dashed lines, provide values for $\rho_n/\rho_p$ which range from 1.7 to 3.4 for the $^{112}$Sn+$^{112}$Sn system (left panel) and 2.8 to 8.2 for the $^{124}$Sn+$^{124}$Sn system (right panel). Statistical models with more accurate treatment of the sequential decay may reduce the uncertainties in these estimates. In all cases, the lower limits of these values are significantly larger than $M$(n)/$M$(p) =1.24 and 1.48 of the initial system marked by arrows in Fig. 3. This confirms that the gas, consisting of free nucleons, contains proportionately more neutrons than the total system. Both the analyses shown in Figs. 2 and 3 indicate a neutron enhancement for the neutron rich system that is roughly twice that of the neutron deficient system.

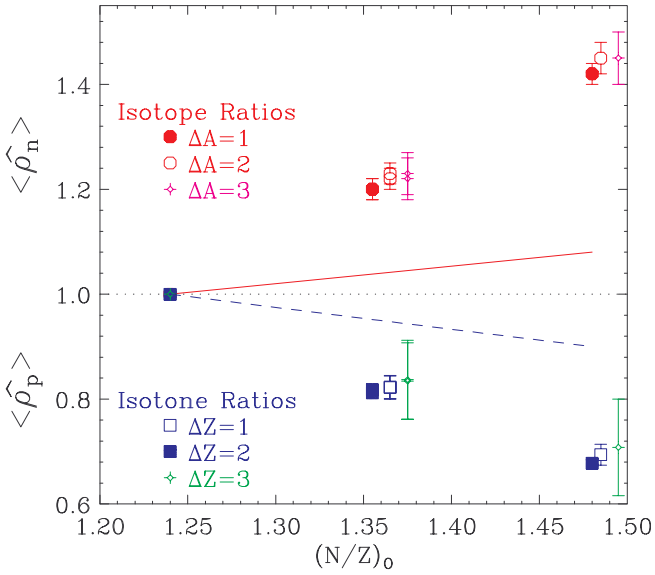


Figure 3: Isobar ratios for three mirror nuclei obtained from the $^{112}Sn+^{112}Sn$ (left panel) and $^{124}Sn+^{124}Sn$ (right panel) reactions. See text for explanation of the lines.

This work is supported by the National Science Foundation under Grant No. PHY-95-28844.

a. NSCL and Department of Physics and Astronomy, Michigan State University, East Lansing, MI 48824, USA.
b. Department of Chemistry and IUCF, Indiana University, Bloomington, IN 47405, USA
c. Department of Chemistry, Washington University, St. Louis, MO 63130, USA

## References

1. L. Phair et al., Nucl. Phys. A **548**, 489 (1992).
2. R.T. de Souza et al., Nucl. Instrum. Methods A **295**, 109 (1990). The Miniwall, a granular extension of the Miniball to forward angles, uses the readout technology of D.W. Stracener et al., Nucl. Instrum. Methods A **294**, 485 (1990).
3. C. Cavata et al., Phys. Rev. **C42**, 1760 (1990); Y.D. Kim et al., Phys. Rev. **C 45,** 338 (1992).
4. G. J. Kunde, et al., Phys. Rev. Lett. 77, 2897 (1996).
5. T. Shimoda, M. Ishihara, K. Nagatani, and T. Nomura, Nucl. Instr. and Methods **165**, 261 (1979).
6. Wagner et al. NSCL Annual Report (1998).
7. J. Randrup and S.E. Koonin, Nucl. Phys. A **356**, 223 (1981).
8. S. Albergo et al., Nuovo Cimento A **89**, 1 (1985).
9. M. B. Tsang, W. G. Lynch, and H. Xi W. A. Friedman, Phys. Rev. Lett. **78**, 3836 (1997).
10. H. Xi et al., Phys. Rev. C **59**, 1567 (1999); H. Xi et al., Phys. Lett B **431**, 8 (1998).
11. V. Viola, K. Kwiatkowski, and W.A. Friedman, Phys. Rev. C **59**, 2660 (1999)
12. G.J. Kunde et al., Phys. Lett. B **416**, 56 (1998).
13. It may be possible for the free proton density to exceed the free neutron density in extremely proton rich systems.
14. A.S. Botvina et al., Nucl. Phys. **A475,** 663 (1987); J.P. Bondorf et al., Phys. Rep. **257,** 133 (1995).
15. W. Tan, private communication and to be published.